Time resolved solvent rearrangement dynamics

Todd Sanford, Django Andrews, Jeff Rathbone, Mark Taylor, Felician Muntean, Matthew Thompson, Anne B. McCoy,† Robert Parson and W. Carl Lineberger*

JILA and Department of Chemistry and Biochemistry, University of Colorado, Boulder, CO 80309, USA

Received 15th December 2003, Accepted 12th January 2004
First published as an Advance Article on the web 19th May 2004

Ultrafast pump–probe studies of I_2^- recombination in size-selected $I_2^-(CO_2)_n$ cluster ions demonstrate long time coherent motions in size-selected clusters and the resulting non-statistical energy flow in the cluster. For I_2^- photodissociated to produce either $I^- + I$ or $I^- + I^*$, we identify a solvent-driven energy transfer process without a condensed phase counterpart. The mechanism involved is a Marcus-like solvent-driven curve crossing, with the driving force arising from asymmetric solvation, not just from solvent orientation. By substituting another halogen for one I atom, we "break" the I_2^- symmetry, and thus obtain direct information on the electron transfer process. New experiments on $IBr^-(CO_2)_n$ photodissociation products confirm the behavior suspected in the I_2^- studies. Time-resolved experiments on IBr^- and theoretical modeling of the dynamics provide quantitative information on the multiple curve crossings encountered in the recombination process. In related investigations, femtosecond negative ion-neutral-positive ion charge reversal apparatus is employed to investigate transient neutral species evolving along a reaction coordinate. We report studies of the rearrangement dynamics of $Cu(OH_2)$ produced by photodetachment of the corresponding anion. Following a controlled delay period, a second ultrafast tunable laser pulse initiates resonant multiphoton photoionization of the time-evolving $Cu\cdots OH_2$ complex. The time-resolved Cu^+ and $Cu^+(OH_2)$ signals provide information both on the prompt dissociation of the complex and on energy redistribution between internal rotational and radial modes of the evolving complex. Calculations of the time evolution of the anion geometric configuration on the neutral potential energy surface yield deeper insight into the nature of the rearrangement process and the energy flow within the complex.

Introduction

The multitude of interactions in which the solvent plays a crucial role affords many opportunities for studies of pathways and mechanisms. Gas phase ionic clusters represent an especially appealing medium for studying effects of solvation. They serve as microsolutions that can simplify the interpretation of observables, and afford the possibility of unraveling the effects of solvation on a microscopic scale. Moreover, the choice of weakly bound ionic chromophores in the microsolvent

† JILA Visiting Fellow, 2003. Permanent Address: Department of Chemistry, Ohio State University, Columbus, OH, USA.

enables both mass selection of the initial species and readily accessible photoinitiation of reactive processes for dissociation.

We have previously reported extensive studies of the caging and recombination dynamics of I_2^- in carbon dioxide[1–4] and carbonyl sulfide solvents,[2,5] including studies of a new type of photofragment caging,[1,6,7] in which the solvent plays an important collective role in quenching spin orbit excited iodine atoms. Theoretical interpretation of the experimental data also predicts[6,7] a strong electron transfer process in which the excess electron in I_2^- is more localized on the less solvated end of the ion. In any event, large-scale motions of the solvent play a critical role in the caging process.

In this work, we explore these electron transfer processes by breaking the symmetry of the I_2^- chromophore, replacing it with ICl^- or IBr^-. Studies of photofragment caging of these asymmetric species lends strong support to the model developed for I_2^-.

In a second set of experiments, solvent reorientation is studied in the metal anion water complexes and shows the importance of solvent reorganization on photodissociation dynamics. In this study, we employ femtosecond pump–probe laser spectroscopy and quantum dynamical calculations to examine the H_2O reorientation and dissociation dynamics within a $Cu(H_2O)$ complex that is produced by photodetachment of $Cu^-(H_2O)$. This experiment exploits the fact that a polar molecule in a binary complex with an atomic metal anion will undergo large-amplitude reorientation and dissociation following electron photodetachment. In all of these experiments, an intimate interplay between theory and experiment gives a much more detailed understanding of the chemistry than either process alone.

2. Experiment

In this section we briefly describe the three types of experiments that will be utilized in these studies: (1) determination of ionic state distributions in visible and near-ultraviolet photodissociation of size-selected $IBr^-(CO_2)_n$ cluster ions; (2) ultrafast pump probe measurements of IBr^- caging in these clusters; and (3) ultrafast photodetachment of a negative ion cluster complex, followed by time delayed multiphoton ionization of the evolving neutral complex.

The tandem time-of-flight ion beam apparatus has been described in detail elsewhere. The $IBr^-(CO_2)_n$ cluster ions are formed by attachment of slow secondary electrons to IBr in an electron impact ionized pulsed supersonic expansion,[8] comprised of He, IBr, and CO_2 gasses. The cluster ions grow by subsequent solvent nucleation about IBr^-. The copper water complexes are formed in a sputter modification of the source,[9,10] in which a copper electrode is sputtered in the high-pressure region at the throat of the supersonic expansion, forming copper anions; subsequently, water molecules are attached to the copper anion. Once the cluster ions are formed, they are mass selected in a Wiley-McLaren time-of-flight mass spectrometer. At this spatial focus, the ion beam is crossed with a beam of pulsed laser radiation synchronized to interact only with ions of the desired mass. The remainder of the apparatus is used for time-of-flight analysis of either the cationic or anionic photoproducts. It includes a second retarding, reflectron mass spectrometer and a microchannel plate detector located at the spatial focus of the reflectron. Using this second reflecting field, we detect either the ionic products of one photon photodissociation of the cluster anions, or the two photon products of the pump–probe experiment on the cluster ions. The time resolution in the pump–probe studies is about 120 fs. Finally, if the potential of the reflectron is reversed, then we are able to detect the mass-selected cationic products derived in the charge reversal experiment. The time resolution in the last experiment degrades to about 250 fs. Further details of these devices are given in other publications.[1–4]

3. Caging in size-selected cluster anions

While the problem of accurate determination of multidimensional potential energy surfaces for clusters is a daunting one, the problems become compounded when we consider the fact that only rarely does chemistry take place on a single potential energy surface. The cage effect and photodissociation dynamics have traditionally been and to date remain a major testing ground for multisurface, nonadiabatic processes. The active role of the solvent in cage recombination was

emphasized by the calculations of Gerber and co-workers[11] showing solvent insertion into the recombining chromophore and the experimental and theoretical studies of Lineberger and co-workers[1,2,4] and Parson and co-workers[6,12–15] showing solvent-driven curve crossings, emphasizing the importance of the solvent field on the recombining chromophore. The interplay between theory, experiment and simulation is nowhere more productive than in these complex, multisurface aggregates. The I_2^- ion has been the favorite chromophore for caging of ionic compounds, and in this section, we study the effects of varying both the symmetry of the ionic chromophore and the nature of the solvent.

The electronic states of I_2^- have been the subject of numerous theoretical and experimental investigations, and a reasonably accurate view of the six lowest lying states of this ion has emerged.[16–18] This set of potentials is shown in the left panel in Fig. 1. Information concerning the disposition of solvents about the chromophore comes from a simple electrostatic/quantum method developed by Faeder and co-workers[19] to obtain structures of the partially solvated ion; these structures show strongly asymmetric solvation about the chromophore, largely because the solvent-solvent bond strength is moderate compared to the ion-solvent bond strength. The recombination events that will be reported here concern excitation to the A′ state of I_2^-, leading to an apparently "simple" curve crossing required to achieve recombination and caging upon excitation to this state. In contrast, excitation to the B $^2\Sigma$ state produces $I^- + I^*$ products and requires approximately one eV spin–orbit quenching collision in order to recombine to the ground state. In order for these processes to occur efficiently, Parson and his students have shown that an electron transfer event is required,[13,14,20] moving charge away from the "solvated" end of the ion in order to facilitate the curve crossing. In either case, very efficient recombination occurs even when the first solvent shell is only partially filled. Thus, Fig. 2 shows the probability of caging I_2^- following excitation to the A′ $^2\Pi$ state for solvent molecules CO_2, OCS and N_2O. In each case, nearly 80% caging is achieved with a degree of solvation such that only one end of the diatomic chromophore is covered with solvent; the caging reaches 100% at roughly the cluster size corresponding to completion of the first solvent shell. Qualitatively similar caging is seen for excitation to the B $^2\Sigma$ state, where spin–orbit de-excitation is also required.

Pump–probe studies of I_2^- recombination as a function of cluster size yield insight into the rate at which these multiple surface crossings take place. Fig. 3 shows the rate of recombination from following excitation to the A′ state as a function of the number of CO_2 solvents around the chromophore.[21] The recombination rate increases steadily with cluster size in the range shown here (from 8–17 CO_2 solvents) and in each case the recombination rates are in the range of 10 ps.

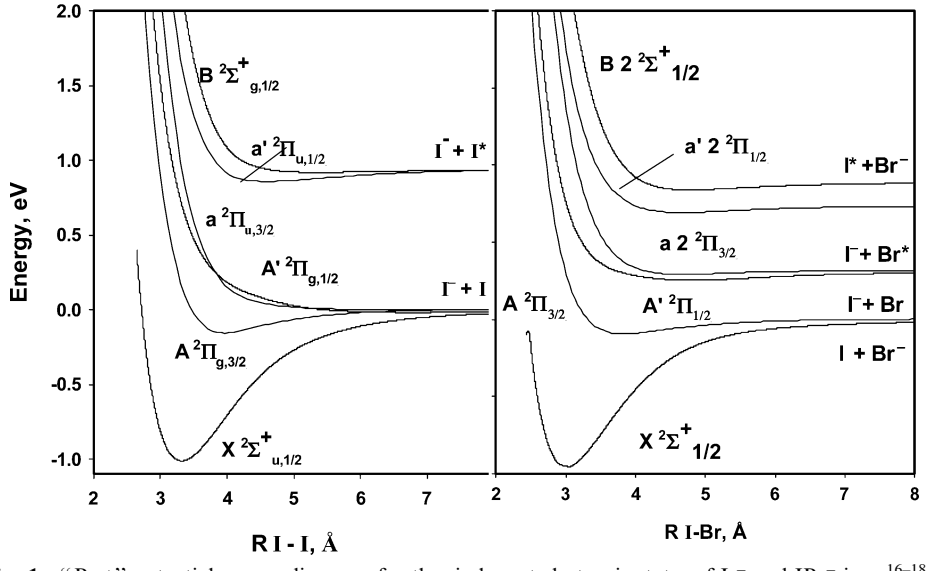

Fig. 1 "Best" potential energy diagrams for the six lowest electronic states of I_2^- and IBr^- ions.[16–18,22]

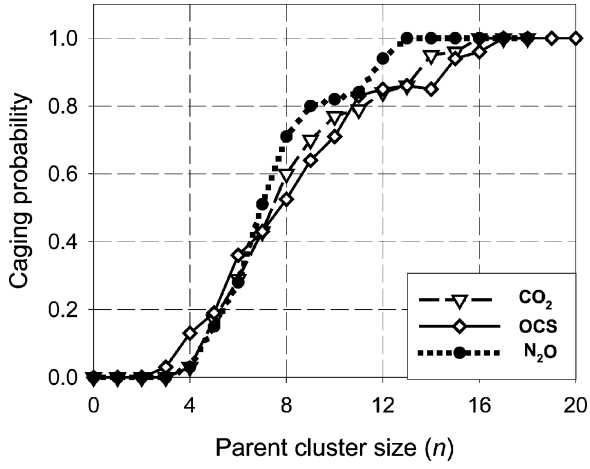

Fig. 2 Caging probability as a function of the number of solvent molecules for $I_2^-X_n$ excited to the A′ $^2\Pi$ state, for several species of solvent. Whether the solvent is primarily bound by dipolar (OCS or N_2O) or quadrupolar (CO_2) interactions, the caging behavior is remarkably similar for excitation to this state.

Similar rapid rates are seen in recombination from following B $^2\Sigma$ excitation, except now both a solvent-driven spin–orbit relaxation and this internal electron transfer must have taken place.

To test these ideas further, we have carried out new experiments in which the nature of the chromophore is changed, altering the symmetries and providing a direct mechanism by which we can test the electron transfer hypothesis. The right panel in Fig. 1 shows an equivalent set of potential energies for the six equivalent low lying states of IBr^-.[22] The fact that the bromide ion is smaller than the iodide ion means that the partially solvated cluster will be predominately solvated about the bromide end, and that thus we will be able to excite to different states of the ion with solvation at different ends.

By breaking the symmetry of the ion, we are able to excite selectively to states that dissociate to "either end" of the molecule, choosing either $I + Br^-$ or $I^- + Br$ products. Photoabsorption experiments carried out in our laboratory have verified the correctness of these potentials, particularly for the A′ $^2\Pi_{1/2}$ state, the analog to the A′ state of I_2^-. In this case, however, excitation to

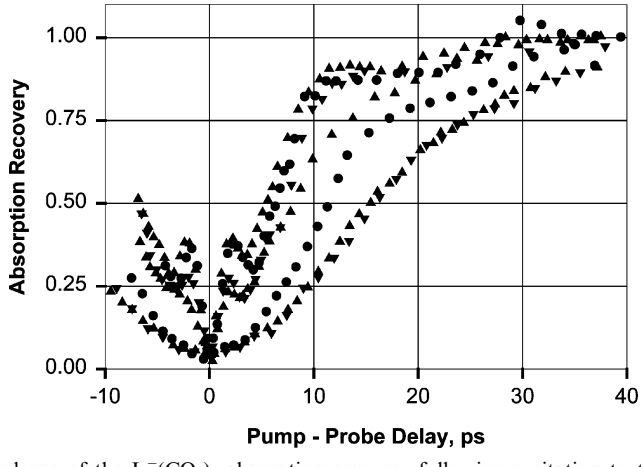

Fig. 3 Time dependence of the $I_2^-(CO_2)_n$ absorption recovery following excitation to the A′ $^2\Pi$ state as a function of the cluster size. The cluster sizes shown here are 8, 9, 12, 14, 16 and 17 CO_2 solvents, with the recovery rate increasing monotonically with the number of solvent molecules. With solvation ranging from half a solvent shell to a full shell, the characteristic absorption recovery time is in the 5–16 ps time frame.[4,21]

the A′ state leads to dissociation to an excited exit channel, $I^- + Br$, located some 0.3 eV above the $I + Br^-$ asymptote.

As a first test of the symmetry breaking, we replace I_2^- with IBr^- and excite to the A′ state. Fig. 4 shows the ionic products of 790 nm photoexcitation of $IBr^-(CO_2)_n$, as a function of the number of CO_2 solvent molecules. When no solvent is present ($n = 0$ in Fig. 4), we observe only an I^- photoproduct verifying that, at this wavelength, we excite only to the $A'\,^2\Pi$ state. As the number of CO_2 solvent molecules is increased, the initial I^- product fraction decreases rapidly, virtually vanishing with four solvent molecules. At this point, there is a very substantial (20%) charge transfer (Br^-) based product and nearly 80% caged products. Representative cluster ion structures [$IBr^-(CO_2)_4$ and $IBr^-(CO_2)_8$] are shown as insets in Fig. 4; these structures emphasize the significant asymmetry of the partially solvated clusters and the fact that the solvents are concentrated near the smaller, Br, end of the IBr^- ion. With the attachment of eight solvent molecules (approximately half of the first solvent shell), *only* caged (IBr^-) clusters are observed as photoproducts. The overall shape of the caging product curve seen in Fig. 4 is very similar to the equivalent I_2^- curve seen in Fig. 2. This picture, however, serves as an unequivocal demonstration of the existence of the charge transfer product, in this case as a transient species as a function of the number of solvent molecules. When similar studies[23] are carried out for ICl^-, as seen in Fig. 5, the caged fraction rapidly increases to 100% with only three solvent molecules, but then the caged fraction equally rapidly approaches zero with eight or nine solvent molecules and leaves only the Cl^- charge transfer product. In this case, the cage transfer completely dominates the caging process with the result that no caging whatever is observed.

The next step in understanding this process is to determine the time scale for the successful caging events. The fact that we detect recombination by detecting recombined photoproducts with fewer solvent molecules attached makes it very difficult to obtain recombination data for chromophores with fewer than about six solvents. Consequently, we have been unable to follow the rate of A′ state recombination for $ICl^-(CO_2)_n$ in the 3–6 cluster size range that would be required to detect a recombined product. As a result, we have carried out absorption recovery measurements on $IBr^-(CO_2)_8$ following A′ state excitation. As can be seen from Fig. 5, at this cluster size the caged fraction is essentially 100% and, based upon the fact that the IBr caged fraction looks so similar to the I_2 caged fraction, we expect again to observe absorption recoveries on a 10 ps time scale. In fact, in this case absorption recovery takes place with the characteristic time of about 6 ns! This result is quite surprising to us, and it appears that it involves some kind of trapping on the A′ state, although eventually there must be recombination to the ground state rather than radiative

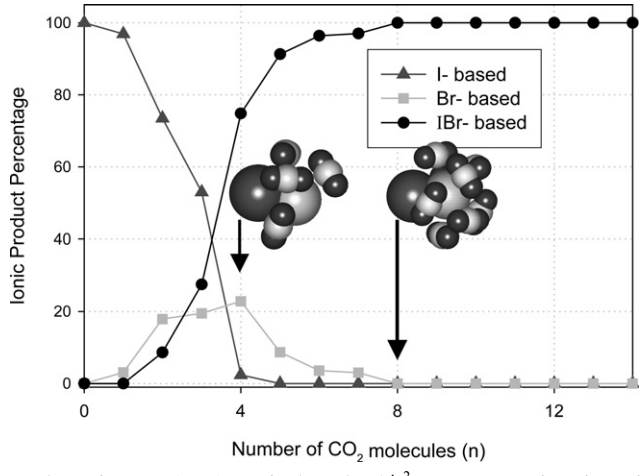

Fig. 4 Ionic photoproducts for $IBr^-(CO_2)_n$ excited to the $A'\,^2\Pi$ state, as a function of the number of CO_2 solvent molecules. The fact that only one product is present for $n = 0$ shows that the 790 nm excitation is able to excite a single state, and the rapid buildup of the Br^- product demonstrates clearly the solvent driven electron transfer.

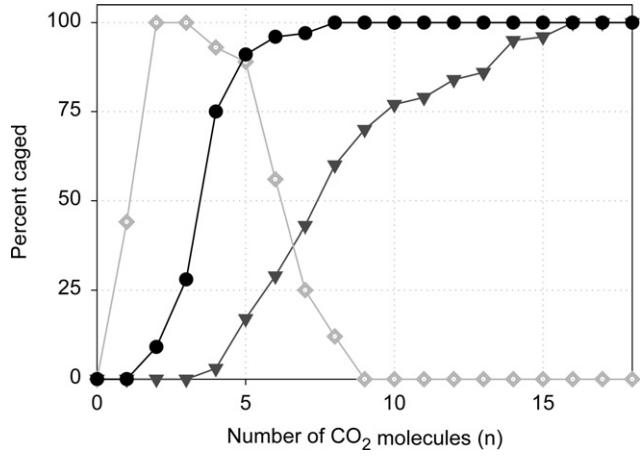

Fig. 5 Caging fraction for several $IX^-(CO_2)_n$ cluster ions as a function of the number of CO_2 solvent molecules, following excitation to the $A'\ ^2\Pi$ state. ● IBr^-; ◆ ICl^-; and ▽ I_2^-. The similar behavior of I_2^- and IBr^- led us to expect similar recombination times for these two chromophores, not what was observed.

transfer, because solvent loss makes it clear that there has not been photoemission. These results encourage us to do a number of further experiments, but significant modeling is going to be required to further understand this multistate process.

While these investigations of dynamics in large cluster ions provide insight into collective solvent effects, it is very difficult to envision experiments that will provide detailed information on individual solvent motions, if indeed such information would prove informative. In part for this reason, we carry out complementary experiments on much smaller cluster ions, specifically ones where we know that there will be large scale solvent reorganization following electron photodetachment. Such experiments on Cu^-H_2O are described in the next section. A major goal of these experiments is to obtain a more detailed view of solvent reorganization following a major change in the charge distribution on the chromophore.

4. Solvent rearrangement dynamics and dissociative photodetachment

The basic idea of this experiment is quite straightforward. When a dipolar molecule forms a weak bond with the anion of an electropositive atom, the positive end of the dipole will point toward the anion. Upon electron detachment, the resulting neutral complex may dissociate, but, if it remains bound, the solvent dipole will undergo both a reversal and a change in distance from the chromophore. This process has been investigated theoretically for the equivalent case of halide–water complexes[24] by Jungwirth and coworkers.[25,26] Our experimental realization of this process[10] involves water attached to a copper anion. The experimental approach is indicated schematically below:

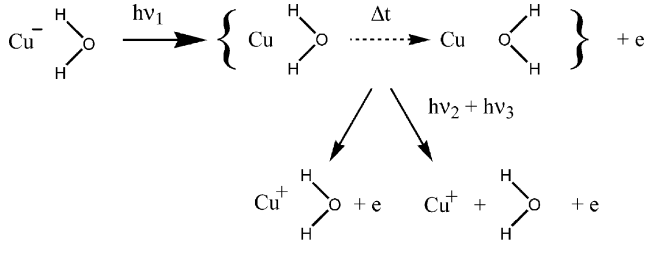

Resonant multiphoton ionization is employed to follow the time evolution of the neutral complex. Several experimental investigations are performed in order to follow the evolution of the $Cu(H_2O)$ complex in its ground electronic state. In all cases, the neutral dynamics are initiated by electron

photodetachment of $Cu^-(H_2O)$ with 398 nm radiation, and the time evolution of the neutral is followed by delayed multiphoton ionization. The ionization schemes all take advantage of the large Cu–H_2O separation in the evolving neutral complex; this separation gives rise to a set of molecular energy levels that resemble those of a Cu atom perturbed by an electric field. In Fig. 6, the various laser pulse sequences employed in these studies are superimposed upon schematic, partial potential energy diagrams for the anion, neutral ground and intermediate excited states, and the cation. The potential energy diagrams show the C_{2V} surfaces with the water hydrogen atoms directed either toward (dashed lines) or away from (solid lines) the copper atom. The wavelengths employed result in product detection windows at large (Scheme 2) to moderate (Schemes 3 and 4) copper-water separations. Different schemes are particularly sensitive to 1) direct dissociation of the complex and 2) longer time dissociation driven by intramolecular vibrational energy redistribution in the evolving complex. These processes are discussed separately in the following sections.

4.1 Direct dissociation and short time dynamics

The initial dynamics of the $Cu(H_2O)$ neutral is suggested by the results of our potential energy surface calculations, as detailed elsewhere.[27] In summary, initiating the neutral dynamics from the $Cu^-(H_2O)$ anion provides a defined initial nuclear configuration with the hydrogen atoms oriented toward the anion and confined to relatively tight angular orientations.[27] By contrast, immediately after electron photodetachment, the region of the neutral potential energy surface that is sampled by the nascent wave packet is close to isotropic, indicating that the H_2O becomes a quasi-free internal rotor in the initially formed $Cu(H_2O)$ neutral. In addition, the constrained angular intermolecular motion of $Cu^-(H_2O)$ anion, especially the out-of-plane bending, upon electron photodetachment converts into significant (internal) rotational excitation of the quasi-free H_2O. An order of magnitude estimate of this excitation is provided by the classical period of rotation of the H_2O moiety. If we assume that half of the zero-point energy[27] of the intermolecular bending

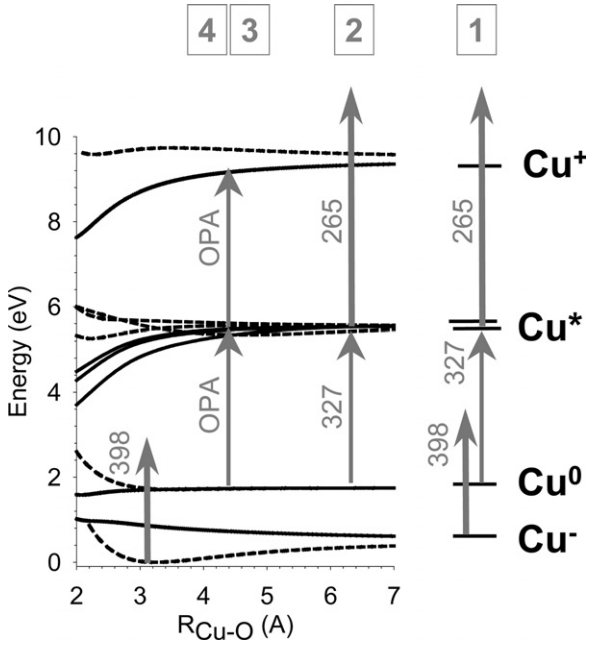

Fig. 6 Schematic representation of the measurements performed. (1) 398 nm photodetachment of Cu^-, followed by two-color (327, 265 nm) resonant ionization of Cu, (2) 398 nm photodetachment of $Cu^-(H_2O)$ followed by two-color (327, 265 nm) resonant ionization of the Cu photofragment, (3) 398 nm photodetachment of $Cu^-(H_2O)$, followed by OPA REMPI (315–345 nm), detecting $Cu^+(H_2O)$, and (4), 398 nm photodetachment of $Cu^-(H_2O)$ followed by OPA REMPI (315–345 nm), detecting Cu^+.

modes of the anion ($\sim$250 cm^{-1}) is converted into rotational kinetic energy of the H_2O in the neutral, for an average rotational constant of 17 cm^{-1} for H_2O, we obtain 0.25 ps for a full rotation and 0.125 ps for water reorientation in the opposite direction. Following the same arguments for the case of $Cu(D_2O)$, a kinetic energy of 203 cm^{-1} and an average rotational constant of 9 cm^{-1} yields a 0.195 ps time for reorientation in the opposite direction for the D_2O moiety. These water reorientation times for both $Cu(H_2O)$ and $Cu(D_2O)$ are shorter than the effective time resolution of our experiment, 0.25 ps, and we do not expect to resolve the reorientation processes in the present experiments.

Fig. 7 shows qualitatively that the total energy of the $Cu(H_2O)$ neutral formed upon photodetachment is comparable to the dissociation energy, so we expect to observe direct dissociation of the complex. More precisely, calculations[27] of the overlaps between the anion ground vibrational state wave function and all of the bound states of the neutral indicate that approximately 1/3 of the initial neutral wave packet will have energies above its dissociation threshold, and this fraction will increase for the vibrationally excited states of the anion. An order of magnitude estimation of the time required for direct dissociation of the ground vibrational state can be calculated from the zero-point energy in the radial intermolecular mode of the anion (50 cm^{-1}) and by assuming a flat potential in the radial direction out, for the neutral. If half of the zero-point energy converts into kinetic energy, the time required for the Cu and (H_2O) to move 4 Å apart (7.3 Å total) is 1.95 ps. This is significantly greater than the 0.6 ps observed,[10] indicating that, rather than the ground state, vibrational excited states contribute primarily to the observed dissociation time. This conclusion is substantiated by the quantum wavepacket calculations of Cu^+ and $Cu^+(H_2O)$ signals, discussed below and in more detail elsewhere.

Short time data, emphasizing the onsets of the two signals in the first 5 ps after electron photodetachment from $Cu^-(H_2O)$, are presented in Fig. 8.[10] The solid line represents the Cu^+ signal from the photodetachment-photoionization of Cu^-, scheme (1) in Fig. 6, and indicates the time resolution of our experiment. The $Cu^+(H_2O)$ signal increases at the same rate, indicating that this ion is initially formed at a rate more rapid than our 250 fs resolution. In contrast, the Cu^+ onset is both resolvable and delayed with respect to the photodetachment event. Weak oscillatory features are observed in the $Cu^+(H_2O)$ signal after very long averaging times. These features will be discussed in a future publication.

Direct dissociation is clearly observed in our experimental signals through the rapid rise of the Cu^+ signal in the first ps after photodetachment (Fig. 8). Fits to the experimental data indicate a time constant of 0.6 ± 0.2 ps for this process. The delayed onset of the Cu^+ signal with respect to

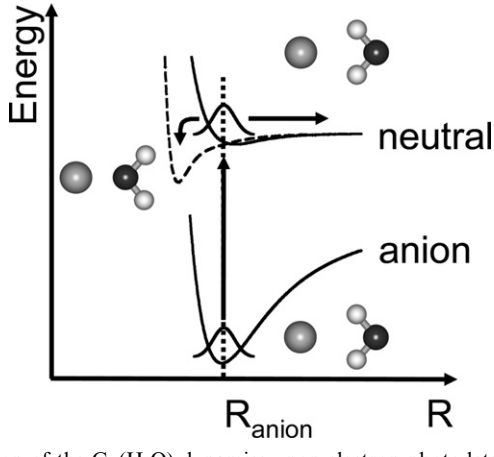

Fig. 7 Schematic illustration of the $Cu(H_2O)$ dynamics upon electron photodetachment of the negative ion. The lines represent potential energy curves along the $Cu^-(H_2O)$radial intermolecular coordinate for the anion and neutral complexes in the two C_{2v} orientations: CuH_2O (solid lines) and $CuOH_2$ (dashed line). The vertical arrow depicts the photodetachment process, and the other arrows suggest the rearrangement (left) and dissociation (right) of the neutral complex following photodetachment.

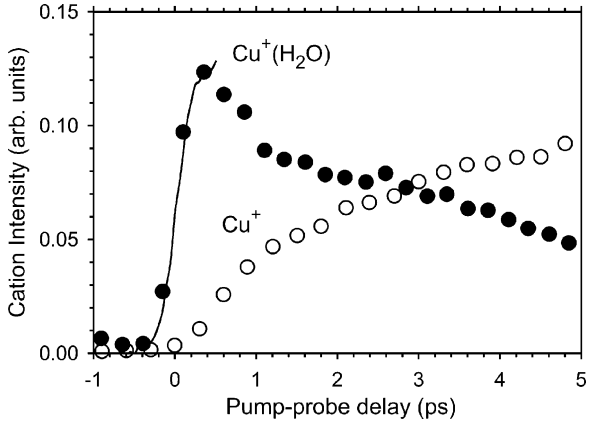

Fig. 8 Experimental time-dependence of the photodetachment-photoionization of $Cu^-(H_2O)$ in the first 5 ps after photodetachment. The Cu^+ signal (white circles) is a result of 398 nm photodetachment followed by two-color (327 + 265 nm) resonant ionization, Scheme (2) in Fig. 6. The $Cu^+(H_2O)$ signal (black circles) is a result of 398 nm photodetachment followed by one-color (327 nm) resonant ionization, Scheme (3) in Fig. 6. The photodetachment-photoionization of Cu^- (solid line) illustrates the *in situ* measurement of the experimental time resolution, 0.25 ps.

the photodetachment is understood as the time required for the wave packet to reach a detection window at large intermolecular separations, which is consistent with photoionizing resonantly the separated Cu atom (327 nm).

The quantum mechanical wave packet propagation calculations[27] offer detailed insight into the initial dynamics of the system. At $\Delta t = 0$, immediately after photodetachment, the wave function is localized in a relatively small angular range of H2O orientations around the anion configuration, with the hydrogens pointing toward Cu as in the equilibrium configuration of the anion.[27] Within 80 fs, the wavepacket is substantially delocalized in these bending coordinates;[27] as this time is less than the experimental resolution, we cannot observe this process. At later times, we can expect to resolve the wavepacket evolution corresponding to the much slower motion along the Cu–H_2O coordinate. Indeed the wavepacket propagations show clearly that only Cu–O stretch vibrations contribute significantly to this initial, direct dissociation and yield dissociation times consistent with observations.[10] The wavepacket propagations over the first 5 ps, shown in Fig. 9, are in remarkably good agreement with the observations.

There is little change in the amount of direct dissociation upon deuteration in both the calculated signals and the experiment, within the uncertainties. The density of bend vibrational states of the anion is larger in the deuterated case, while the density of stretch states is approximately the same.

4.2 Dissociative photodetachment of $Cu^-(H_2O)$

In these experiments, we investigate the process of dissociative photodetachment of $Cu^-(H_2O)$ by monitoring both the increase of the Cu atom fragment concentration and the decreased population of the $Cu(H_2O)$ complex as a function of time following photodetachment. The Cu atom photofragment is detected with a sequence of 327 and 265 nm pulses, producing Cu^+ and labeled (2) in Fig. 6. While the 327 nm radiation is resonant with the separated Cu atomic $^2P_{\frac{1}{2}} \leftarrow {}^2S_{\frac{1}{2}}$ transition, the bandwidth of the 327 nm pulse results in excitation of the Cu–H_2O complex at any separation in excess of ~ 6 Å. The portion of the initially bound $Cu(H_2O)$ complex that evolves to large Cu–H_2O separation is detected by a one-color atomic resonant (327 nm) multiphoton ionization producing Cu^+H_2O, process (3) in Fig. 6. This molecular detection window is only open for a restricted radial separation, because two 327 nm photons (7.58 eV) can ionize the bound $Cu(H_2O)$ complex in restricted water orientations and they have insufficient energy to ionize the isolated Cu atom (IP = 7.73 eV).

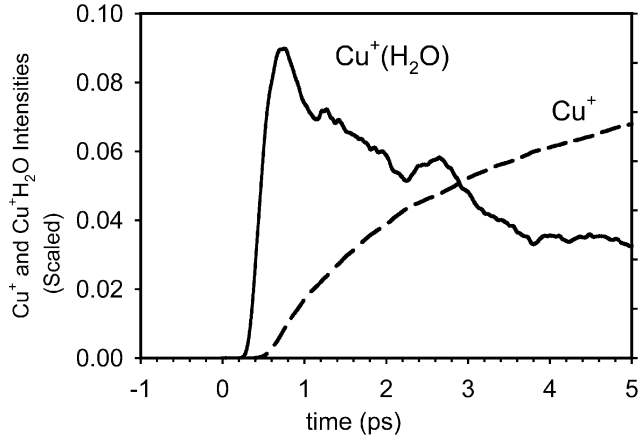

Fig. 9 Calculated probabilities of detecting Cu^+ and $Cu^+(H_2O)$ cation signals as a result of quantum mechanical wave packet propagation calculations.[27] The curves represent the results of propagation on the neutral potential energy surface of the 10 lowest energy vibrational wave functions of the $Cu^-(H_2O)$ anion, with an assumed anion temperature of 150 K. The ionization detection windows employed are 5.5–7 Å for $Cu^+(H_2O)$ and >7 Å for Cu^+.

The time dependence of the Cu^+ cation signal for 100 ps after electron photodetachment from $Cu^-(H_2O)$ is presented in Fig. 10. The Cu^+ signal rises rapidly during the first picosecond, then more slowly for the next several ps. The Cu^+ signal continues to rise at an even slower rate, and is still increasing slowly after 100 ps, exhibiting at least three distinct dissociation time scales during the 100 ps observation period.

The $Cu^+(H_2O)$ signal, also shown in Fig. 10, exhibits a complementary behavior.[10] It rises rapidly and decays over >10 ps, and the decay cannot be described by a single exponential. We note from Fig. 10 that the Cu^+ and the $Cu^+(H_2O)$ signals are related. The sum of the two signals is a constant function of the photodetachment-photoionization delay time, an indication that the two signals have similar characteristic time-constants at time longer than 5 ps. This verifies the fact that the Cu^+ signal observed originates from the dissociation of the $Cu(H_2O)$ neutral complex, followed by resonant ionization of the Cu atom.

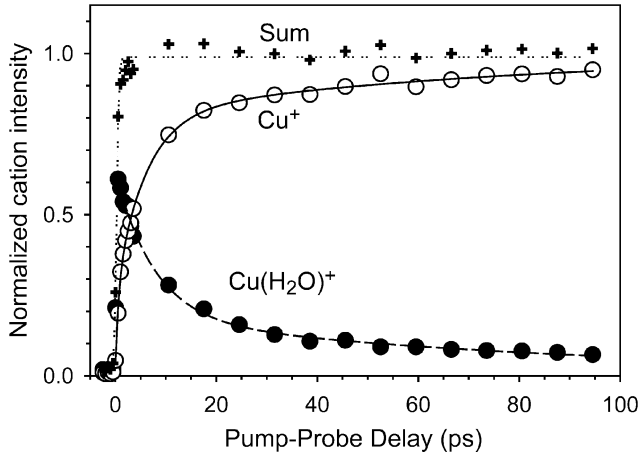

Fig. 10 Experimental time-dependence of the photodetachment-photoionization of $Cu^-(H_2O)$. The Cu^+ signal (white circles) is a result of 398 nm photodetachment, followed by two-color ($327+265$ nm) resonant ionization, Scheme (2) in Fig. 5. The $Cu^+(H_2O)$ signal (black circles) is a result of 398 nm photodetachment followed by one-color (327 nm) resonant multiphoton ionization, Scheme (3) in Fig. 5. The weighted sum (crosses) of the two signals is presented along with a constant line fit (dotted line) to this sum.

Inspection of the intermediate state(s) in Fig. 6 shows that changing the OPA wavelength slightly from the 327 nm Cu atom resonant transition in turn moves the excitation window to smaller Cu–H_2O separation. When the second photon absorbed by the neutral complex is also an OPA photon, ionization is energetically possible only for restricted angular orientations of the water molecule. Thus detecting $Cu^+(H_2O)$ formed by absorption of two OPA photons arises from photoabsorption in a restricted angular and radial range, as depicted in process (3) in Fig. 6. The corresponding Cu^+ signals arise from dissociative multiphoton ionization of $Cu(H_2O)$, process (4) in Fig. 6. Such experiments were carried out, detecting the ionic products following excitation at 315, 331, 335, 340, and 345 nm. A similar measurement using the more intense, but non-resonant, 265 nm third harmonic radiation was also attempted, but no cation signals above background levels were detected.

The $Cu^+(H_2O)$ transient signals obtained at excitation wavelengths between 315 nm and 345 nm, but avoiding the 327 nm Cu resonance transition, show no significant differences (within the experimental scatter) from the 327 nm excitation data shown in Fig. 10. However, the Cu^+ ions are no longer the result of resonant excitation, are much weaker, and have the same time dependence as the $Cu^+(H_2O)$ cation. The reason is that the on resonance Cu^+ signal arises from Cu atoms produced *dissociative photodetachment* of $Cu^-(H_2O)$, while the off resonance Cu^+ arise from *dissociative multiphoton photoionization* of CuH_2O. The $Cu^+/Cu^+(H_2O)$ ratio increases with decreasing excitation wavelength, indicating that the $Cu^+(H_2O)$ dissociation fraction increases with increasing energy of the photoionization photons.

5. Summary and conclusions

In an effort to understand the role of electron transfer in dihalide ion recombination, we have investigated the recombination of $IBr^-(CO_2)_n$ cluster ions following excitation to the $A'\ ^2\Pi_{1/2}$ state. The cage fraction behaves very much as has been observed for I_2^-, and the ability to identify the iodide or bromide ionic products conclusively establishes the electron transfer process implicated in earlier I_2^- studies. The IBr^- recombination rate, however is at least two orders of magnitude slower than observed for I_2^-. In order to obtain more detailed information on individual solvent molecule motions, we have subsequently carried out a study of a smaller cluster ion, Cu^-H_2O, using a photodetachment- resonant multiphoton ionization approach. A combination of experiment, *ab initio* electronic structure calculations and fully quantum wavepacket calculations has given new insight into the short time solvent motions in this system.

Acknowledgements

We gratefully acknowledge support from the National Science Foundation under Grants CHE0201848 and PHY0096822 (W.C.L.) and CHE-0200968 (A.B.M.), and the Air Force Office of Scientific Research Grant F49620-02-1-0371 (W.C.L.). A.B.M. was supported by the JILA Visiting Fellowship program.

References

1 A. Sanov, T. Sanford, S. Nandi and W. C. Lineberger, *J. Chem. Phys.*, 1999, **111**, 664.
2 S. Nandi, A. Sanov, N. Delaney, J. Faeder, R. Parson and W. C. Lineberger, *J. Phys. Chem. A*, 1998, **102**, 8827.
3 J. M. Papanikolas, V. Vorsa, M. E. Nadal, P. J. Campagnola, H. K. Buchenau and W. C. Lineberger, *J. Chem. Phys.*, 1993, **99**, 8733.
4 J. M. Papanikolas, P. J. Campagnola, V. Vorsa, M. E. Nadal, H. K. Buchenau, R. Parson and W. C. Lineberger, *The Chemical Dynamics and Kinetics of Small Radicals*, 1995, **6**, 616.
5 A. Sanov, S. Nandi and W. C. Lineberger, *J. Chem. Phys.*, 1998, **108**, 5155.
6 N. Delaney, J. Faeder and R. Parson, *J. Chem. Phys.*, 1999, **111**, 651.
7 N. Delaney, J. Faeder and R. Parson, *J. Chem. Phys.*, 1999, **111**, 452.
8 M. A. Johnson and W. C. Lineberger, *Techniques for the Study of Ion Molecule Reactions*, 1988, 591.
9 D. W. Boo, Y. Ozaki, L. H. Andersen and W. C. Lineberger, *J. Phys. Chem. A*, 1997, **101**, 6688.
10 F. Muntean, M. S. Taylor, A. B. McCoy and W. C. Lineberger, *J. Chem. Phys.*, 2004, in press.
11 A. Cohen, M. Y. Niv and R. B. Gerber, *Faraday Discuss.*, 2001, **118**, 267.

12 J. Faeder and R. Parson, *J. Chem. Phys.*, 1998, **108**, 3909.
13 N. Delaney, J. Faeder and R. Parson, *J. Chem. Phys.*, 1999, **111**, 651.
14 N. Delaney, J. Faeder and R. Parson, *J. Chem. Phys.*, 1999, 651.
15 J. Faeder, N. Delaney, P. E. Maslen and R. Parson, *Chem. Phys. Lett.*, 1997, **270**, 196.
16 P. E. Maslen, J. Faeder and R. Parson, *Chem. Phys. Lett.*, 1996, **263**, 63.
17 M. T. Zanni, T. R. Taylor, B. J. Greenblatt, B. Soep and D. M. Neumark, *J. Chem. Phys.*, 1997, **107**, 7613.
18 M. T. Zanni, V. S. Batista, B. J. Greenblatt, W. H. Miller and D. M. Neumark, *J. Chem. Phys.*, 1999, **110**, 3748.
19 J. Faeder, N. Delaney, P. E. Maslen and R. Parson, *Chem. Phys.*, 1998, **239**, 525.
20 J. Faeder, N. Delaney, P. E. Maslen and R. Parson, *Chem. Phys. Lett.*, 1997, **270**, 196.
21 J. M. Papanikolas, PhD Thesis, University of Colorado, 1994, p. 240.
22 M. Thompson and R. Parson, to be published, 2004.
23 M. E. Nadal, P. D. Kleiber and W. C. Lineberger, *J. Chem. Phys.*, 1996, **105**, 504.
24 W. H. Robertson and M. A. Johnson, *Annu. Rev. Phys. Chem.*, 2003, **54**, 173.
25 M. Roeselova, M. Mucha, B. Schmidt and P. Jungwirth, *J. Phys. Chem. A*, 2002, **106**, 12 229.
26 M. Roeselova, U. Kaidor and P. Jungwirth, *J. Phys. Chem. A*, 2000, **104**, 6523.
27 M. S. Taylor, F. Muntean, A. B. McCoy and W. C. Lineberger, *J. Chem. Phys.*, 2004, in press.